INVESTIGATING MAGNETIC CONTROLLED REACTOR PRINCIPLES AND CHARACTERISTICS UTILIZING ANSYS IN AN IN-DEPTH STUDY

Samuel Addo **DARKO**[1], Edmund Kwafo **ADJEI-SAFORO** [1,2], Misbawu **ADAM**[1], Solomon Nchor **AKANSAKE**[2]

[1] *Kumasi Technical University,* [2]*Kwame Nkrumah University of Science and Technology, kingacid17@gmail.com, adam.misbawu@kstu.edu.gh*

Keywords: Magnetic controlled reactor (MCR), core structure, magnetic field distribution, magnetic saturation

Abstract*: The inherent complexity leads to intricate equations, making it challenging for design engineers and researchers to model and analyze MCRs effectively. Despite the increasing attention given to MCRs in power systems, the need for simplified theoretical foundations and design models persists. This paper addresses the challenges posed by the complex excitation conditions of magnetic controlled reactors (MCRs), which are subject to both alternating current and direct current excitations by presenting the theoretical basis, ontological structure, working principle, and design model of MCRs in a systematic manner for enhanced comprehension. Graphical and equivalent electric circuit approaches are employed to derive mathematical expressions, while ANSYS simulation is utilized to create a 3D structure model of the MCR. The simulation results, compared with theoretical analyses, demonstrate that the MCR exhibits alternate magnetization and demagnetization between its two core limbs in a cycle. This suggests that the magnetic valves on both sides alternate between saturation and unsaturation in each cycle. Furthermore, the research reveals that the MCR's entire capacity can be smoothly adjusted by varying the saturation degree of the magnetic valve core. Overall, this research contributes to a deeper understanding of MCRs under actual operating conditions and serves as a crucial foundation for further investigations into their performance design.*

1. INTRODUCTION

Although transformers are inevitable in power generation, power transmission and power distribution stations, in recent years, however, MCR has also become one of the most

essential equipment used in long distance EHV and UHV transmission lines, as well as substations with high voltage fluctuations, because of its good control flexibility, high reliability and simple maintenance [1] [2] [3] [4]. MCR is a type of reactive power compensation equipment which can reduce grid losses, eliminate generator self-excitation, control power frequency over-voltage, limit short-circuit current and control operations automatically [5] [6] [7]. Currently, more than 8 GVA of total reactor capacity have been successfully installed around the world in various voltage buses, from 10 to 500 kV and still counting [8] [9]. On the basis of that, there are currently considerable worldwide research activities all over the world especially, Russia, America, Germany, United Kingdom, Brazil and China.

From the early 1950s, General Electric Company of England installed more than fifty magnetic controlled reactors with the capacity from few to hundreds MVA in electric grids of different countries [10]. However, due to economic and technical performance limitations, such as high material cost, low speed, limited control range and low power efficiency, manufacturing of these machines were brought to a halt. In 1971, H. Becker studied on the first three-phase three-winding magnetic controlled reactor model which the magnetic iron core legs have cylindrical winding [11]. Many modern designs of MCR can be traced as a prototype of his construction. A suggestion was also made by him that MCR would be useful for compensating reactive power. In the 1980s, Alma-Ata University in USSR investigated and developed more prototypes. In the year 1990 to 1992 at Zaporozhye Transformer Factory (ZTR) in collaboration with V.I.Lenin All-Soviet Electrotechnical Institute built a full-scale 500 kV / 60 MVA single-phase MCR and successfully put into test at a high-voltage test facility near Moscow, Russia. Since then, many different capacities have been designed and produced, including the first commercialized 60 MVA / 500 kV 3-single-phase units in 2005, and the first three-phase 180 MVA unit in 2009 [12]. In September 2007, China Electric Power Research Institute cooperated with Shenyang Transformer Factory also proudly produced the first 120 MVA / 500 kV magnetic controlled reactor in China, which was successfully put into operation at Jiang Ling Converter Substation [13]. In June 2013, the three-phase 110 MVA / 750 kV magnetic controlled reactor developed by TBEA Shen Chang Company was also successfully put into operation at Qinghai Yuka Switch Station.

MCR is mostly designed either a single-phase or three-phase, where its cooling system can be air type or oil-immersed type depending on the application it is subjected to. Its technical core involves ferromagnetic material characteristics, magnetic circuit design, nonlinear theory, AC and DC co-excitations and control system characteristics. Along with its good developmental trend, simplification in modeling and analysis has become more and more difficult, deterring new and young researchers to dive into.

This paper thoroughly analyzes MCR's theory, provides simplified mathematical calculations and establishes a 3D MCR prototype model in ANSYS Maxwell. Hence, providing convenience for design engineers and research works as a whole.

2. THE CORE STRUCTURE AND WORKING PRINCIPLE

2.1. Core structure and winding configurations

The configuration of the Magnetic Controlled Reactor (MCR) resembles that of a transformer but functions on the principle of a magnetic amplifier. Its adaptability has led to various core structures and connections. *Fig. 1* and *2* depict the typical core structure and winding arrangements for a single-phase MCR, featuring an iron core with magnetic valves, working winding, and control winding [14].

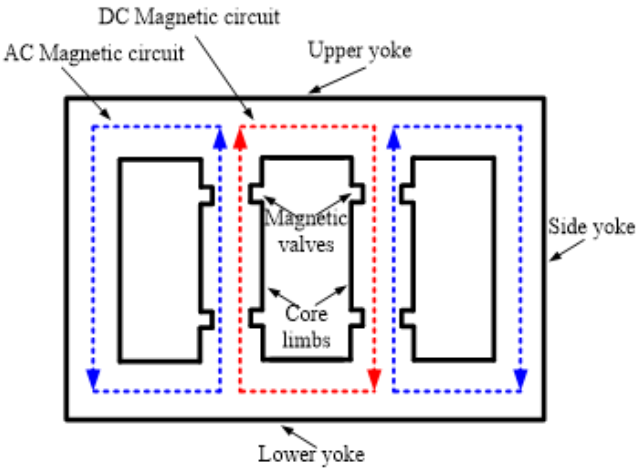

Fig. 1. Core structure of a single phase MCR

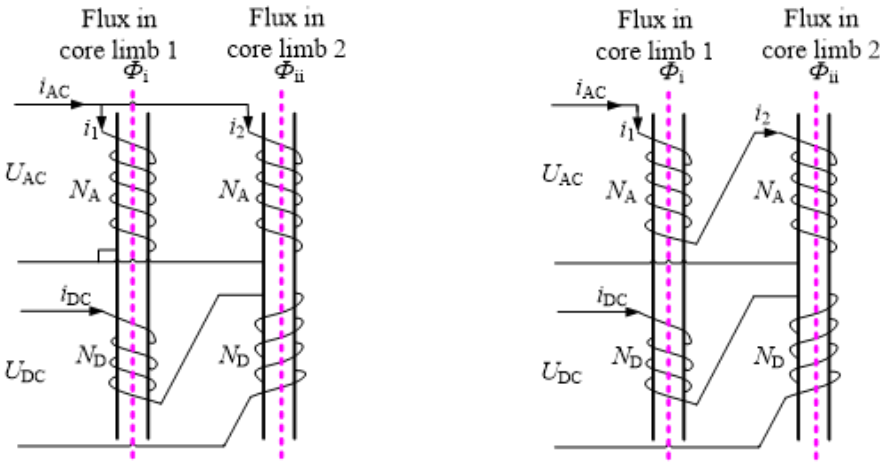

(a) Working winding in parallel *(b) Working winding in series*

Fig. 2. Winding arrangements

The iron core comprises two parallel limbs and two side yokes, offering a closed-loop path for magnetic flux during excitation [15]. Both working and control winding are affixed to the core limbs, with N_A representing the number of working winding turns and N_D representing

the number of control winding turns [16] [17]. U_{DC} represents a DC source of voltage that creates DC current I_{DC} flowing within the control winding which induces DC magnetic flux in the core limb *i* and core limb *ii* with an equal magnitude but opposite direction [18]. The working winding are sometimes referred to as AC winding because their terminals are directly connected in parallel to the power network and control winding are also referred to as DC winding because their terminals are connected to DC source where the MCR is being controlled [19]. The DC winding are wired in reverse-series so that the fundamental component of the voltages is annihilated. This helps to minimize the insulation of the equipment and achieve a better level in control characteristics [20].

To achieve control over the magnetic saturation in Magnetic Controlled Reactors (MCRs), both the winding connection and magnetization characteristics play crucial roles. When the DC control excitation current is nil, the inductance L of the working winding is maximized, and the current in these winding is minimized. This scenario characterizes the MCR as functioning equivalently to the ideal operation of a transformer [21]. However, as the DC bias excitation current starts flowing and gradually intensifies in the control winding, the current in the working winding also proportionally increases. This implies that variations in the control current lead to changes in the magnetic saturation level of the iron core. Consequently, the magnetic permeability of the core fluctuates, allowing precise adjustment of the impedance value of the MCR in accordance with the formula [22]:

$$X = \omega L = \omega \frac{\mu_0 \mu_r N_A^2 A_c}{l_c} \tag{1}$$

where $\omega = 2\pi f$ is the angular frequency, A_c is the cross sectional area of the iron core, l_c is the effective length of the magnetic circuit, μ_0 is the vacuum permeability, μ_r is the relative permeability of the core material and N_A is the winding turns.

2.2. Ferromagnetic materials and magnetizing curve of MCR

Ferromagnetic materials are key elements in all instances of generation, transmission, and conversion of electrical energy. They have great technological and social value, far beyond their mere economic significance [23]. The characteristics of ferromagnetic materials play a very essential role as long as MCR is a concern, because they determine how the saturable core will behave. The magnetic properties of the iron core material determine the performance of the magnetic device and are the basis for the analysis and calculation of magnetic devices. At the same time, the properties of magnetic devices are also largely related to the structure, shape, size and manufacturing process of iron cores. At present, the ferromagnetic materials that are widely used in the area of saturable reactors can be grouped into the following three parts according to their properties and chemical composition [24]:

(1) Silicon steel sheet is mainly used in power frequency high power reactor and power transformers.

(2) High conductivity magnetic nickel alloy is mainly used in magnetic amplifiers, DC current transformers, magnetic modulators, power transformers with special requirements and low power sensitive high frequency pulse saturable reactor.
(3) Ferrite is commonly used for high frequency and pulse excitation components.

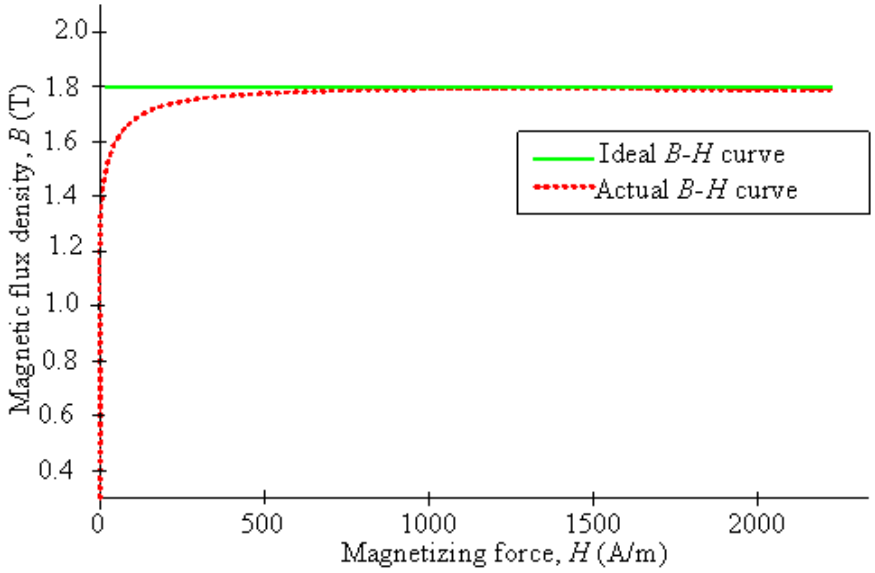

Fig. 3. Magnetization curve of ideal and actual model

The basic magnetizing curve of the silicon steel sheet used for MCR and its ideal magnetizing curve is shown in *fig. 3*. Where the solid green line represents the ideal model and the dot red line represents the actual DC magnetizing curve. However, it should be noted that the core magnetic material used in this paper is the B30G130 grain-oriented magnetic steel sheet type, which its data was published by Wuhan Iron and Steel Mining Company. Moreover, the characteristics and magnetization curves of many different kinds of ferromagnetic materials are presented in detail in literature [23] [25] [26]and [27].

2.3. Magnetic valve of MCR

2.3.1. Characteristics of magnetic valve

Magnetic controlled reactor is said to have a magnetic valve if the core magnetic path is made up of a large area (A_c), (length l_c) and a small area (A_v), (length l_v) in series. Essentially, the magnetic valve can easily be saturated with a small DC bias when has a small area, which of course can greatly save cost. Because the iron core in the large area is always in the unsaturated linear region, the entire capacity of the MCR is determined by changing only the saturation degree of the magnetic path in the magnetic valve [28]. The greater the DC bias, the higher the saturation degree of the valve, and the smaller the equivalent inductance of the MCR. In addition, the magnetic valve can contribute to the mitigation of harmonics when it is carefully designed [29].

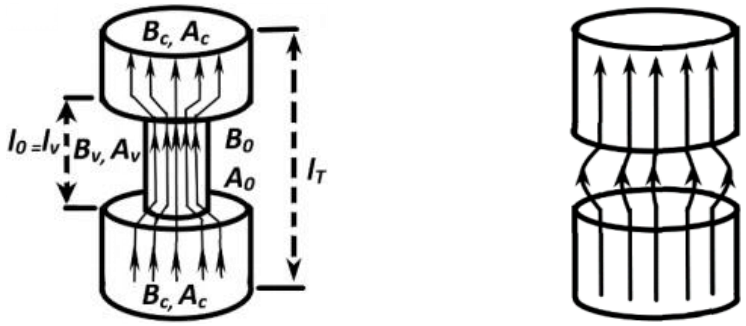

(a) Magnetic valve unsaturated *(b) Magnetic valve fully saturated*

Fig. 4. Characteristics of magnetic valve

Fig. 4 shows unsaturated and saturated characteristics of the magnetic valve. Where l_T is the length of the core limb (m), A_c is the core limb cross-sectional area (m^2), B_c is the core limb flux density (T), l_v is the valve length, A_v is the valve cross-sectional area (m^2), B_v is the valve flux density (T), l_0 is the air-gap length, A_0 is the air-gap cross-sectional area (m^2) and B_0 is the air-gap flux density (T). In *fig. 4(a),* under unsaturated condition, the iron core cross sections, A_v and A_c are in the unsaturated linear zone, and almost all the magnetic lines of force pass through the iron core. The magnetic reluctance is at a minimum and the magnetic valve is said to be fully open. At this point MCR is equivalent to a no-load transformer. In *fig. 4(b)* under saturated condition, only the iron core cross-section, A_v is fully saturated, and its permeability is very small and close to the permeability of the air gap. The reluctance is at a maximum and the magnetic valve is said to be almost close. At this point, the MCR is said to be operating at its maximum design capacity. In other cases where the condition lies in between unsaturated and fully saturated, part of the magnetic lines will pass through the air gap with an area of A_0. The other part of the magnetic line will pass through the magnetic valve, A_v. The magnetic reluctance of A_0 is linear, but that of A_v is non-linear.

2.3.2. Magnetic circuit and equations of magnetic valve

According to Ampere's law relating to current in the coil or turns of wire, the magnetic field created by current following any path is the integral of the fields due to segments along the path. And Faraday's law relating to the voltage applied across the inductor can be expressed in (2):

$$\left.\begin{aligned} F = NI = \oint \vec{H} \cdot d\vec{l} = Hl \\ \vec{B} = \mu\vec{H} = \frac{\mu NI}{l} \\ \emptyset = BA = \frac{\mu NIA}{l} \\ LI = \emptyset N \\ L = \frac{\mu N^2 A}{l} \\ \Re = \frac{l}{\mu A} = \frac{l}{\mu_0 \mu A} \\ L = \frac{N^2}{\Re} \end{aligned}\right\} \quad (2)$$

where H is the magnetic field intensity, $\Re$ is the magnetic reluctance, N is the number of winding, l is the length of the magnetic path (m), A is the magnetic cross-sectional area (m^2), $\mu = \mu_0\mu_r$ is the permeability of the medium (H/m), and μ_0 is the permeability of air, $4\pi \times 10^{-7}$ (H/m), μ_r is the relative permeability and Φ is magnetic flux. The magnetic path of the MCR can be equivalent to the series-parallel circuit shown in f*ig. 5* can be expressed in (3).

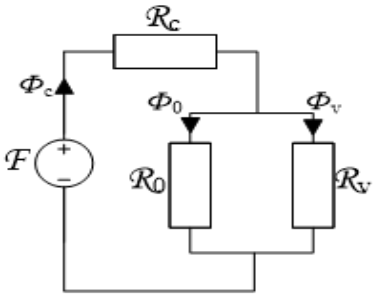

Figure 5. Equivalent circuit (including $\Re_c$)

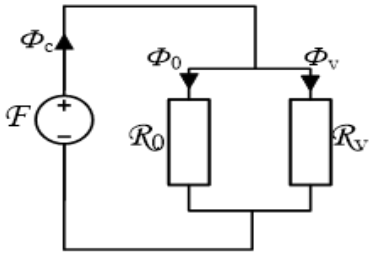

Figure 6. Equivalent circuit (excluding $\Re_c$)

$$\Re_t = \Re_c + \frac{\Re_0 \Re_V}{\Re_0 + \Re_V} \tag{3}$$

where Φ_c is the core limb magnetic flux, Φ_0 is the air gap magnetic flux and Φ_v is the valve magnetic flux, $\Re_c$ is the magnetic reluctance in the core limb, $\Re_0$ is the magnetic reluctance in the air gap, $\Re_V$ is the magnet c reluctance in the valve. From Equation (3), magnetic reluctance $\Re_c$ can be ignored as shown in *fig. 6*, for the reason being that the iron core in the large segment is always in the unsaturated linear region within the entire adjustment range of the MCR, as a result, its magnetic reluctance is much smaller than the magnetic valve segment reluctance [30]

$$\Re_t = \frac{\Re_0 \Re_V}{\Re_0 + \Re_V} \tag{4}$$

It can be seen from (4) that if saturation degree across magnetic-valve can be smoothly changed in the purpose of adjusting the reluctance, then its reactive power can be adjusted accordingly to achieve flexible continuous regulation of output power of the power network.

Now, when the small sectional area of the iron core is in saturation state, and the fringing effect shown in *fig. 4(b)* is neglected, then equations is as below [30]:

$$\emptyset = A_C B = A_0 B_0 + A_V B_V \tag{5}$$

The equation (6) can be obtained through equation (5).

$$B = \frac{A_0}{A_C} B_0 + \frac{A_V}{A_C} B_V \tag{6}$$

Since the small sectional area of iron core and air-gap have the same magnetic field intensity $f(B_v)$, B_0 can be written as:

$$B_0 = \mu f(B_V) \tag{7}$$

Substituting equation (7) into equation (6), B is given by:

$$B = \frac{A_0}{A_C}\mu_0 f(B_V) + \frac{A_V}{A_C}B_V \tag{8}$$

According to the supposition of small slope magnetization curve, when $B_V \leq B_{Vsat}$, the magnetic field intensity of the small sectional area of the iron core $f(B_v) = 0$, then B is expressed as [30]:

$$B = \frac{A_V}{A_C}B_V \tag{9}$$

So, the magnetic field intensity of the equivalent iron core is zero in $0 \leq B \leq (A_V/A_C)B_{Vsat} = B_{sat}$ range. On the other hand, when $B_V \geq B_{Vsat}$, the small sectional area of iron core is then saturated, so magnetic field intensity is expressed as:

$$H = \frac{B_V - B_{Vsat}}{\mu_0} \tag{10}$$

Substituting equation (8) into equation (10), the magnetization curve model of MCR is given in equation (11). And its magnetization curve is presented in *fig. 7*.

$$H = f(B) = \begin{cases} \frac{B+B_{sat}}{\mu_0} & B < -B_{sat} = -\frac{A_V}{A_C}B_{Vsat} \\ 0 & -B_{sat} \leq B \leq B_{sat} = \frac{A_V}{A_C}B_{Vsat} \\ \frac{B-B_{sat}}{\mu_0} & B > B_{sat} = -\frac{A_V}{A_C}B_{Vsat} \end{cases} \tag{11}$$

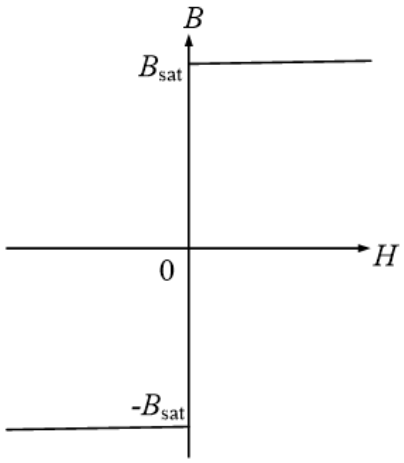

Fig. 7. Ideal core magnetization curve

2.4 Magnetic field analysis of MCR under excitation

To simplify the analysis, the working winding resistance of the magnetically controlled shunt reactor is ignored. Again, it is assumed that the MCR is connected to the power supply with a sinusoidal voltage, $U_{AC} = U_{max} \sin \omega t$. The basic equations of the MCR can be expressed as follows [31]:

$$\begin{cases} \mu_{AC} = E_{max} \sin(\omega t) = A_V N_A \left(\frac{dB_i}{dt} + \frac{dB_{ii}}{dt}\right) \\ U_{DC} = R_D i_{DC} + A_V N_D \left(\frac{dB_i}{dt} - \frac{dB_{ii}}{dt}\right) \\ l_i H_i = i_{AC} N_A + i_{DC} N_D \\ l_{ii} H_{ii} = i_{AC} N_A - i_{DC} N_D \\ H_i = f(B_i) \\ H_{ii} = f(B_{ii}) \end{cases} \tag{12}$$

According to *fig. 2*, the induced EMF in the control winding can be obtained as:

$$U_{DC} = U_{Di} - U_{Dii} = A_V N_D \left(\frac{dB_i}{dt} - \frac{dB_{ii}}{dt}\right) \tag{13}$$

And the induced EMF in the working winding can also be obtained as:

$$U_{AC} = U_{Ai} - U_{Aii} = A_V N_A \left(\frac{dB_i}{dt} + \frac{dB_{ii}}{dt}\right) \tag{14}$$

where U_{Di} and U_{Dii} are the induced EMFs in the control winding while U_{Ai} and U_{Aii} are the induced EMFs in working winding on core I and II, respectively.

Since the working state of the two core structures and winding arrangements are symmetrical, the corresponding magnetic flux density should have the following relationship:

$$\begin{cases} B_i(\omega t) = -B_{ii}(\omega t + \pi) \\ B_{ii}(\omega t) = -B_i(\omega t + \pi) \end{cases} \tag{15}$$

When there is no DC current in the control winding, thus $I_{DC} = 0$, $B_{DC} = 0$, as well, and the AC magnetic flux density B_i, B_{ii} varies only between $-B_{sat}$ and $+B_{sat}$, and the amplitude is$B_{max} = B_{sat}$. Now, increasing the DC bias excitation in the control winding increases the DC component in B_i, B_{ii}, so that their top rises (drops) beyond the $+B_{sat}$ ~ $-B_{sat}$ range as shown in *fig. 8*.

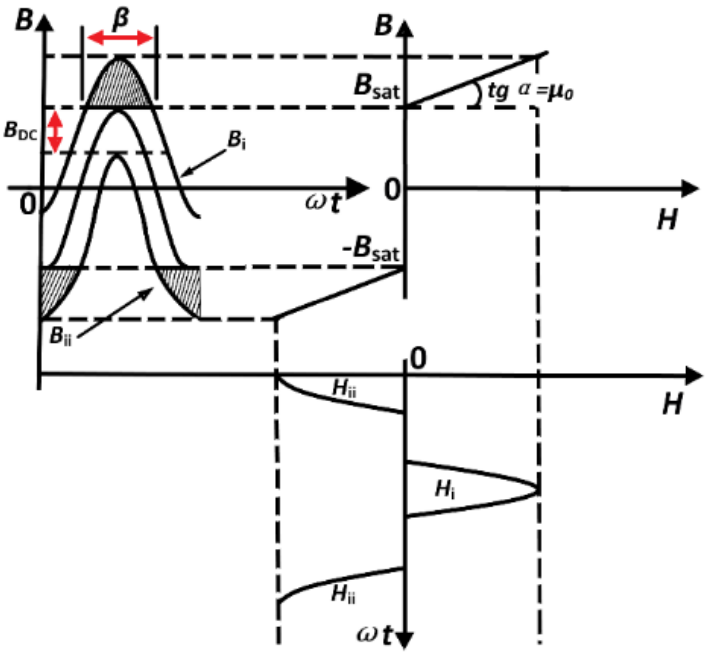

Fig. 8. DC bias core magnetic saturation schematic diagram

The horizontal axis portion corresponding to the shaded portion in the *fig.* (electrical angle is 2β) indicates the core saturation time of the half core limb in the power frequency for one cycle and is expressed by β, which is called magnetic saturation. In the theoretical analysis of MCR, a magnetic saturation β plays a very essential role. When the control current is zero, B_{DC} = 0, the half core limb is not saturated in a complete power frequency cycle, so $\beta = 0$. As the control current increases, the saturation time of the half core limb in one cycle increases. When the half core limb is fully saturated in one complete cycle, the magnetic saturation, $\beta = 2\pi$. At this moment, β reaches the maximum limit. Therefore, the magnetic saturation β reflects the degree of saturation of the core, and its values vary from 0 to 2π. Ignoring the effect of flux density harmonics, magnetic saturation can be obtained from Equation (16).

$$\beta = 2arcos\left(\frac{B_{sat}-B_{DC}}{B_{sat}}\right) \tag{16}$$

And DC flux density is

$$B_{DC} = B_{sat}\left[1-\cos\left(\frac{\beta}{2}\right)\right] \tag{17}$$

Through the corresponding B-H curve, the magnetic field strength of the core limb I and II can be obtained as follows:

When

$$\left(\pi-\frac{\beta}{2}\right) \le \omega t \le \left(\pi+\frac{\beta}{2}\right)$$

$$H_i = \frac{B_{sat}}{\mu_0}\left(-\cos\omega t-\cos\frac{\beta}{2}\right) \tag{18}$$

But when

$$0 \le \omega t < \frac{\beta}{2} \text{ or } \left(\pi + \frac{\beta}{2}\right) < \omega t \le 2\pi$$

$$H_i = 0$$

$$0 \le \omega t < \frac{\beta}{2} \text{ or } \left(2\pi - \frac{\beta}{2}\right) < \omega t \le 2\pi$$

$$H_{ii} = \frac{B_{sat}}{\mu_0}\left(-\cos \omega t - \cos\frac{\beta}{2}\right) \tag{19}$$

But when

$$\frac{\beta}{2} \le \omega t \le \left(2\pi - \frac{\beta}{2}\right)$$

$$H_{ii} = 0$$

If the working current of MCR is given as $i_{AC} = \frac{l}{2N_A}(H_i + H_{ii})$, then the amplitude of current fundamental component is:

$$i_{ACn} = \frac{2}{\pi}\int_0^{\pi} i_{AC} \cos \omega t \, d\omega t = \frac{2}{\pi}\int_0^{\pi} \frac{l}{2N_A}(H_i + H_{ii}) \cos \omega t \, d\omega t$$

$$= \frac{lB_{sat}}{\pi\mu_0 N_A}\int_{\pi-\frac{\beta}{2}}^{\pi}\left(-\cos \omega t - \cos\frac{\beta}{2}\right) \cos \omega t \, d\omega t + \int_0^{\frac{\beta}{2}}\left(-\cos \omega t + \cos\frac{\beta}{2}\right) \cos \omega t \, d\omega t$$

$$i_{ACn} = \frac{lB_{sat}}{2\pi\mu_0 N_A}(\beta - \sin \beta) \tag{20}$$

The working current of MCR reaches maximum at $\beta = 2\pi$ is:

$$i_{AC\,max} = \frac{lB_{sat}}{\mu_0 N_A} \tag{21}$$

It is realized from Equation (21) that the maximum working current of the MCR depends only on the effective length of the magnetic circuit, magnetic flux density, winding turns and vacuum permeability.

On the other hand, if the control current is $i_{DC} = \frac{l}{2N_A}(H_i - H_{ii})$, then the amplitude of control current fundamental component is:

$$i_{DCav} \approx \frac{1}{\pi}\int_0^{\pi} i_{DC}\, d\omega t = \frac{l}{2\pi N_A}\left[\int_0^{\pi}(H_i + H_{ii})\ d\omega t\ \right]$$

$$\frac{lB_{sat}}{2\pi\mu_0 N_A}\int_{\pi-\frac{\beta}{2}}^{\pi}\left(-\cos\omega t - \cos\frac{\beta}{2}\right)\ d\omega t - \int_0^{\frac{\beta}{2}}\left(-\cos\omega t + \cos\frac{\beta}{2}\right)\ d\omega t$$

$$= \frac{lB_{sat}}{\pi\mu_0 N_A}\left(\sin\frac{\beta}{2} - \frac{\beta}{2}\cos\frac{\beta}{2}\right) \tag{22}$$

The control current of MCR reaches maximum at $\beta = 2\pi$ is:

$$i_{DC\,max} = \frac{lB_{sat}}{\mu_0 N_A} \tag{23}$$

2.5 Harmonic characteristics of MCR

The magnetic controlled reactor takes advantage of the saturation of the small cross-sectional area of the core and the nonlinearity of the core magnetization curve. The working region must be in the nonlinear region; therefore, it will inevitably produce harmonics [32]. It should be noted that the core saturation corresponding to the capacity of the MCR is the rated magnetic saturation, which is β_n. The harmonic characteristics of MCR are analyzed by comparing the maximum value of each harmonic current with the rated fundamental current in the range of the reactor capacity. The calculation of the maximum value of each harmonic wave at$0 \le \beta \le 2\pi$ is shown in Equation (16), in which the base value is the maximum value of the rated fundamental current.

$$\begin{cases} I_{1m}^{*} = \frac{1}{2\pi}(\beta - \sin\beta) \\ I_{(2n+1)m}^{*} = \frac{1}{2\pi(2n+1)}\left[\frac{\sin n\beta}{n} - \frac{\sin(n+1)\beta}{n+1}\right] \\ (n = 1,2,3,\dots) \end{cases} \tag{24}$$

The harmonic current distribution of the magnetic controlled reactor is shown in *fig. 9* using Equation (24). The curves of the per-unit value of fundamental wave, 3rd, 5th and 7th harmonic current with saturation β calculated by Equation (24) are also shown in *fig. 9*. It is clear from the *fig.* that the nth harmonic component of the current of the MCR has n zero points and (n-1) extreme points. Each extreme point is symmetrically distributed with $\beta = \pi$

as the center, and the maximum extreme points of each harmonic are all close to $\beta = \pi$. Again, the whole capacity of the MCR, the maximum content of the total harmonic is not more than 8%. It can also be observed that the maximum amplitude of the 3rd harmonic is about 6.89% of the rated fundamental current, the maximum amplitude of the 5th harmonic is about 2.52%, and the maximum amplitude of the 7th harmonic is about 1.29%, respectively. The distortion coefficient of the current waveform will be smaller because the maximum value of each harmonic wave is staggered.

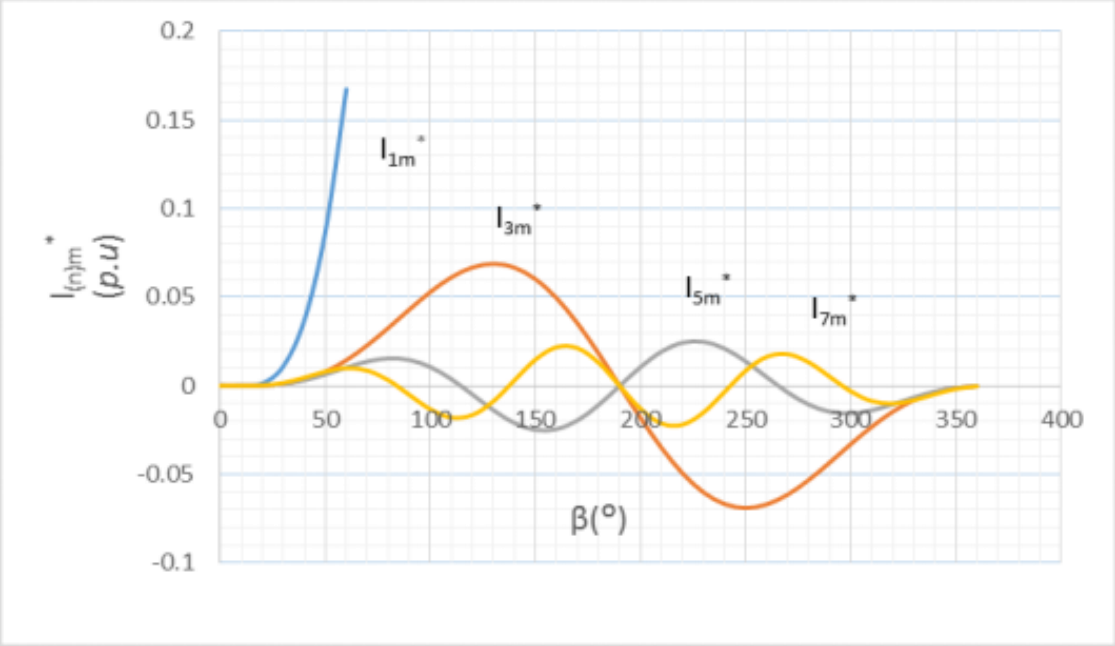

Fig. 9. Harmonic current distribution of MCR

2.6 Equivalent Circuit of MCR

Under rated sinusoidal power supply voltage, the relationship between the amplitude of the fundamental current and the change of the control angle α of MCR is called control characteristics [33]. To control the DC bias excitation current in the control winding, the thyristor control angle needs to be adjusted. So, by adjusting the thyristor angle, however, we can control the added DC bias excitation current to vary the unsaturated regions to change their degree of saturation. Therefore, the magnitude of MCR excitation current depends on the control angle. The smaller the angle, the greater the excitation current, and the magnetization intensity of the unsaturated region and the saturated region is enhanced at the same time. In this way, the reactance value can be continuously and smoothly adjusted. By increasing the DC excitation current, the speed of excitation can be improved, and the dynamic performance of MCR becomes better.

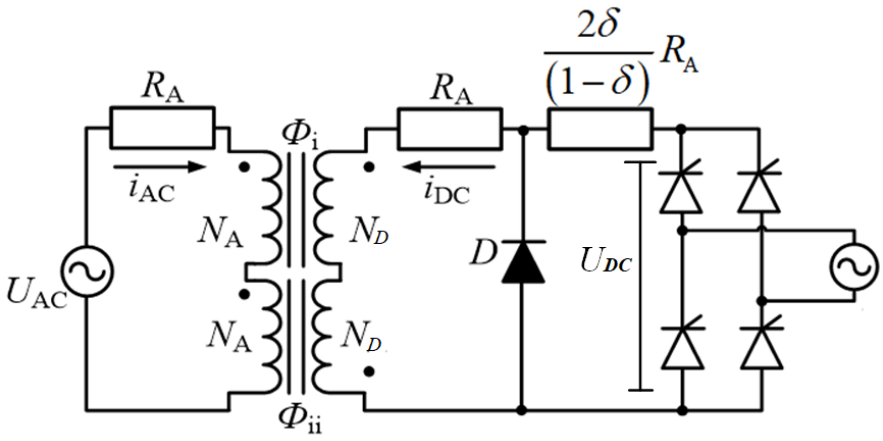

Fig. 10. MCR equivalent circuit

2.6.1 Relationship between control angle and magnetic saturation

The relationship between the control angle α and the saturation β can be obtained from the electromagnetic equation of MCR. From the equivalent circuit in *fig. 10*, if the internal resistance $\frac{2\delta}{1-\delta}R_A$ of the power supply is ignored, and the control angle of MCR is α, then the DC component of control voltage U_{DC} can be derived:

$$U_{DC} \approx \frac{1}{\pi}\int_{\alpha}^{\pi}\frac{\delta E_{max}\sin\omega t}{1-\delta}d\omega t = \frac{\delta E_{max}(1+\cos\alpha)}{\pi(1-\delta)} \tag{25}$$

Where R_A is the winding resistance, E_{max} is the maximum working voltage, α is the control angle of the thyristors and tap ratio $\delta = N_D/N_A$, is the factor which is determined by varying range of reactance in MCR and is usually in between 0.015 to 0.05. A suitable selection of δ can make the wave form better, harmonic components small of the reactor current [33].
By $U_{DC} = i_{DC}R_A$, considering the equations (22) and (25) are:

$$U_{DC} = \frac{\delta E_{max}(1+\cos\alpha)}{\pi(1-\delta)} = \frac{lB_{sat}R_A}{\pi\mu_0 N_A}\left(\sin\frac{\beta}{2} - \frac{\beta}{2}\cos\frac{\beta}{2}\right) \tag{26}$$

When the control angle $\alpha = 0$, the saturation $\beta = 2\pi$, substituting into Equation (26) is:

$$U_{DC\,max} = \frac{2\delta E_{max}}{\pi(1-\delta)} = \frac{lB_{sat}R_A}{\mu_0 N_A} \tag{27}$$

The relationship between the control angle α and the saturation β can be obtained by combining the above two Equations (26) and (27):

$$\cos\alpha = \frac{2}{\pi}\left(\sin\frac{\beta}{2} - \frac{\beta}{2}\cos\frac{\beta}{2}\right) - 1 \tag{28}$$

The relationship between control angle and magnetic saturation using Equation (28) can be obtained graphically as shown in *fig. 11.* The observation result is relatively intuitive. As a matter of engineering practice, the core magnetic saturation β can be obtained according to the fundamental reactive current value I_{1m}, and then the control angle of thyristor α can be calculated.

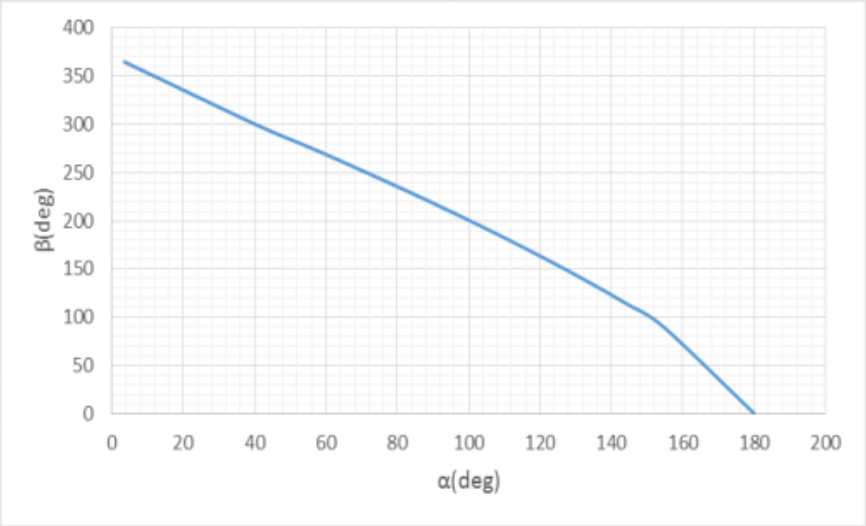

Fig. 11. Relationship between trigger conduction angle and magnetic saturation

2.6.2 Relationship between control angle and working current

When the control angle α of the thyristor changes, the core magnetic saturation degree changes, and then the inductance changes, thereby leading to the adjustment of the working current. The combination of Equations (24) and (28) can be used to obtain the relationship curve of the control angle α and I_{1m}^* of the thyristor in the magnetic controlled reactor, as shown in *fig. 12*. It can be seen that there is an obvious nonlinear between the current value and the control angle of the MCR, and it is an approximate cosine relationship.

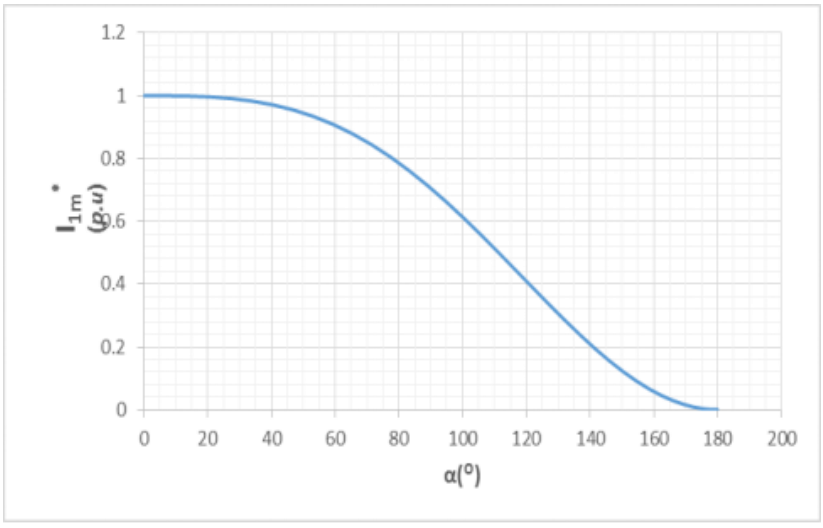

Fig. 12. Control characteristic curve of MCR

The average output voltage of the single-phase controlled rectifier bridge type shown in *fig .10* is:

$$U_{DC} = i_{DC}\left(R_A + \frac{2\delta}{1-\delta}R_A\right) \tag{29}$$

From Equations (27) and (29), at steady state, the average control current i_{DC} can be written as:

$$i_{DC} = \frac{\delta E_{max}(1+\cos\alpha)}{R_A\pi(1-\delta)} \tag{30}$$

Equating Equations (22) and (30) will yield:

$$U_{DC} = \frac{\delta E_{max}(1+\cos\alpha)}{R_A\pi(1-\delta)} = \frac{lB_{sat}R_A}{\pi\mu_0 N_A}\left(\sin\frac{\beta}{2} - \frac{\beta}{2}\cos\frac{\beta}{2}\right) \tag{31}$$

Therefore, control current amplitude of MCR when the control angle $\alpha = 0$, the saturation $\beta = 2\pi$:

$$i_{DC} = \frac{2\delta E_{max}}{R_A\pi(1+\delta)} \tag{32}$$

Combining Equations (23) and (31) is:

$$\frac{2\delta E_{max}}{R_A\pi(1-\delta)} = \frac{\pi l B_{sat}}{\mu_0 N_A} \tag{33}$$

Combining Equations (20) and (31), average working current is:

$$i_{ACn} = \frac{\delta E_{max}}{R_A\pi^2(1-\delta)}(\beta - \sin\beta) \tag{34}$$

Therefore, the working current amplitude of MCR when the control angle = 0 , and the saturation $\beta = 2\pi$:

$$i_{ACm} = \frac{2\delta E_{max}}{R_A\pi(1+\delta)} \tag{35}$$

It is evident from Equation (35) that the working current amplitude of the MCR does not depend only on the applied voltage, but also on the winding resistance and tap ratio. Combining Equations (21) and (35), we obtain:

$$\frac{2\delta E_{max}}{R_A\pi(1+\delta)} = \frac{lB_{sat}}{\mu_0 N_A} \quad (36)$$

Therefore, tap ratio δ can also be written as:

$$\delta = \frac{\pi l B_{sat} R_A}{(2\mu_0 N_A E_{max}) - \pi l B_{sat} R_A} (37) \quad (37)$$

This is to say that, when designing the MCR, the effective length of the magnetic circuit, the flux density of the core material, winding resistance, winding turns and rated voltage should satisfy Equation (37) else, there is a possibility that the magnetic controlled reactor will not function properly.

3. SIMULATION MODEL OF MCR AND RESULTS

3.1. Simulation

The dimensions and specifications of the magnetic controlled reactor used for the simulation are shown in Table 1. A 3D model shown in *fig. 13* is successfully designed using ANSYS. The 3D simulation calculation was adopted in this paper over the 2D because of its high accuracy of simulation results, howbeit it can take an appreciable time. The method of transient solution is also applied because it simultaneously has AC and DC sources. As shown in the simulation circuit (*fig. 14*), the excitation source uses voltage source in place of the current source, because the use of the current source will produce excessive harmonics in the working winding that will seriously affect the current waveform which is not consistent with the actual waveform. The magnetic field distribution, magnetic saturation degree, winding currents and control angle are mainly obtained with a varied control voltage of 0 V to 6.12 V. *fig. 15* to *fig. 24* show the simulation results of the MCR under the same control voltage. Furthermore, the numerical values are presented in Table 2.

Table 1. Dimensions and specifications of the MCR

Parameter		Numerical Value
Total Winding Turns	N_A	194
Control Winding Turns	N_D	6
Winding Resistance (mΩ)	R_A	320
Valve Cross-Section (mm^2)	A	1408
Valve Length (mm)	l	10
Magnetic flux density (T)	B_{sat}	1.8
DC Voltage (V)	U_{DC}	6.12
AC Voltage (V)	U_{AC}	220
Frequency (Hz)	f	50

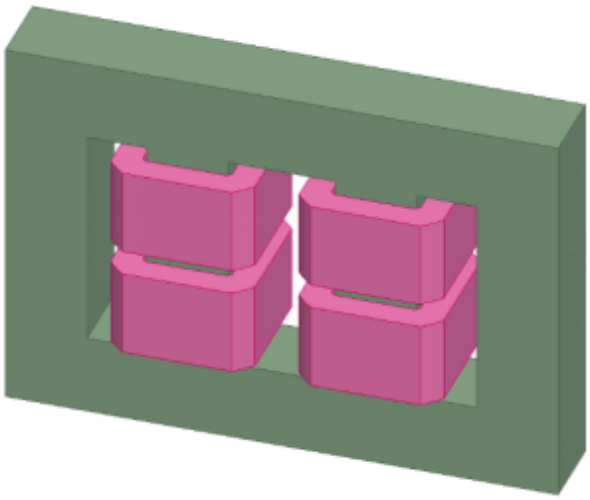

Fig. 13. 3D simulation model of MCR

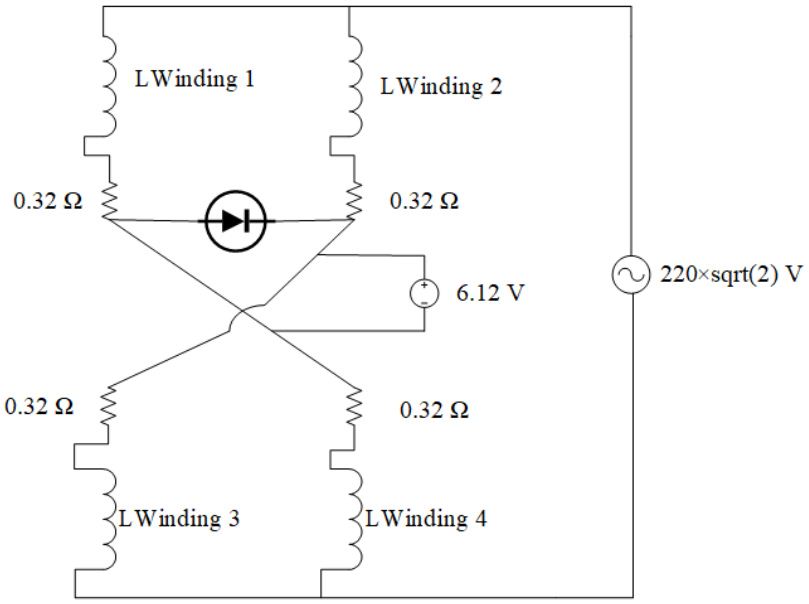

Fig. 14. Simulation circuit of MCR

3.2 Simulation results

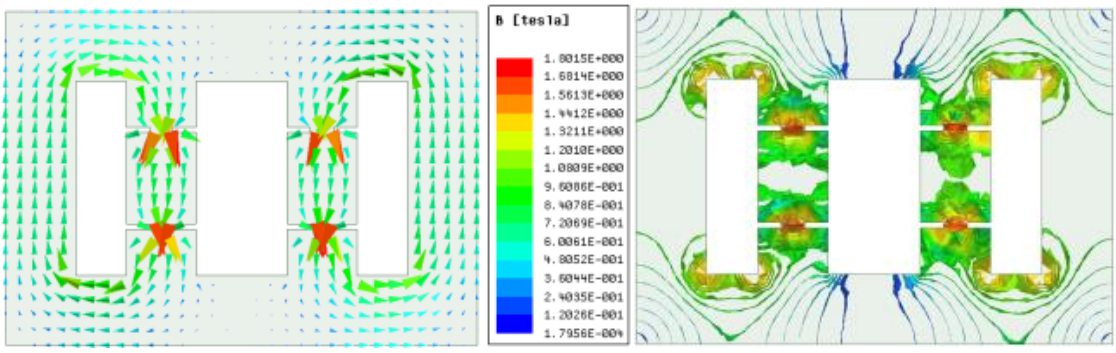

(a) Magnetic flux direction *(b) Magnetic flux density*

Fig. 15. Magnetic flux distribution of MCR in a cycle at t = 9.99s

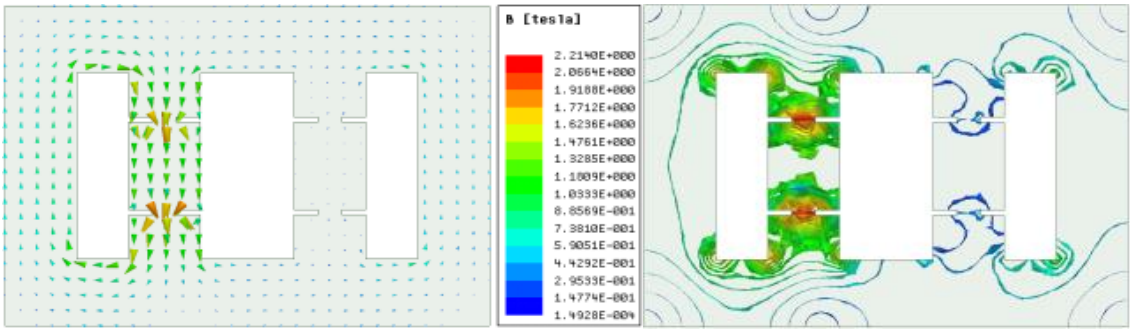

(a) Magnetic flux direction (b) Magnetic flux density

Fig. 16. Magnetic flux distribution of MCR in a cycle at t = 3.389s

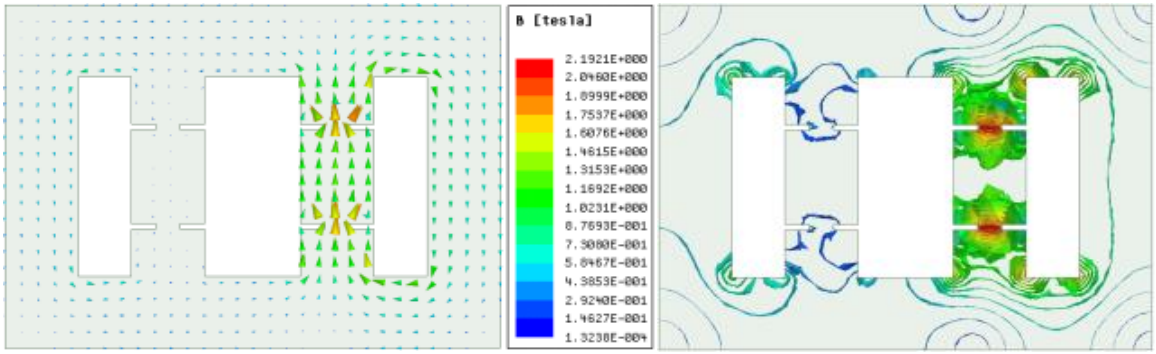

(a) Magnetic flux direction (b) Magnetic flux density

Fig. 17. Magnetic flux distribution of MCR in a cycle at t = 3.399s

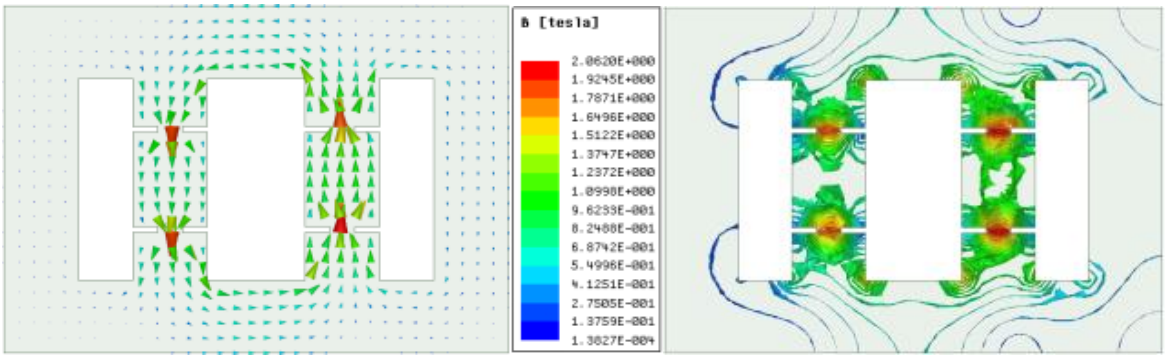

(a) Magnetic flux direction (b) Magnetic flux density

Fig. 18. Magnetic flux distribution of MCR in a cycle at t = 3.355s

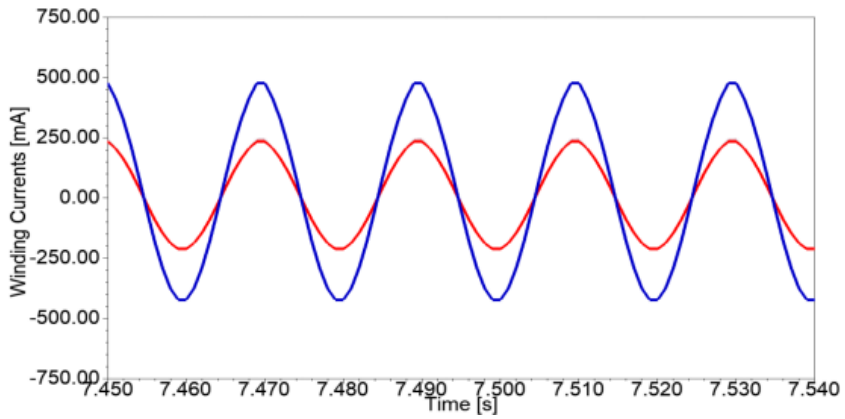

Fig. 19. Simulation results at $U_{DC} = 0\ V$ and Windings current waveform at steady state i_1, i_2 (red line) and i_{AC} (blue line)

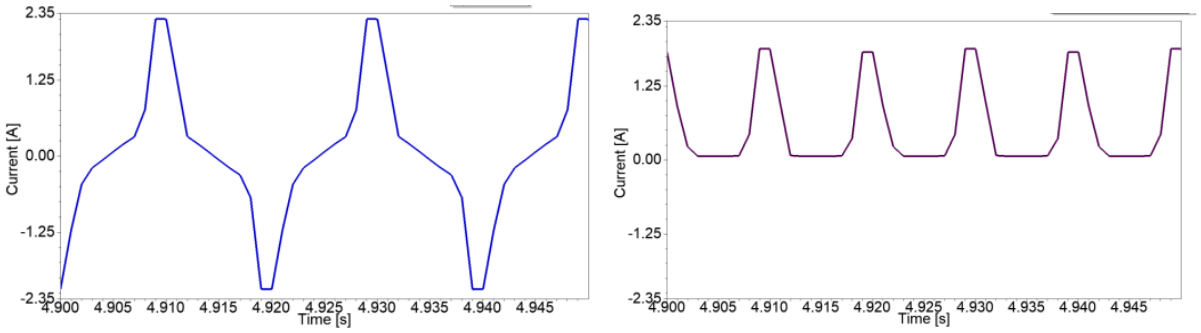

(a) Working current waveform at steady state (i_{AC}) *(b) Control current waveform at steady state (i_{DC})*

Fig. 20. Simulation results at U_{DC}=0.19 V

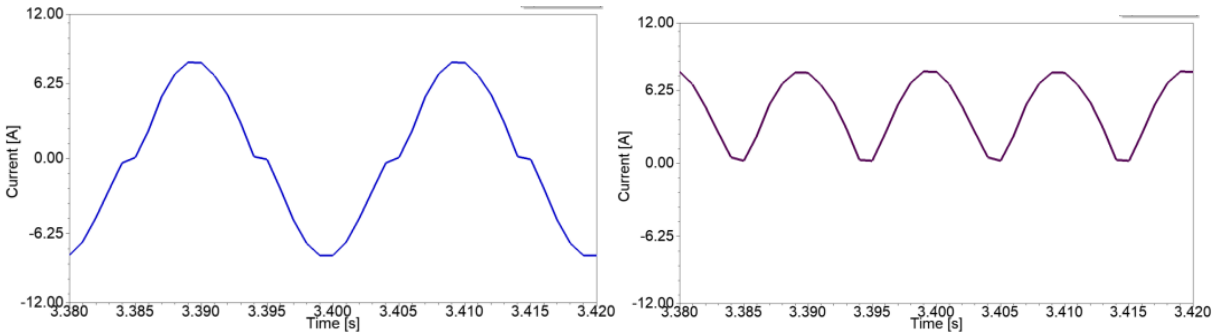

(a) Working current waveform at steady state (i_{AC}) *(b) Control current waveform at steady state (i_{DC})*

Fig. 21. Simulation results at U_{DC}=1.53 V

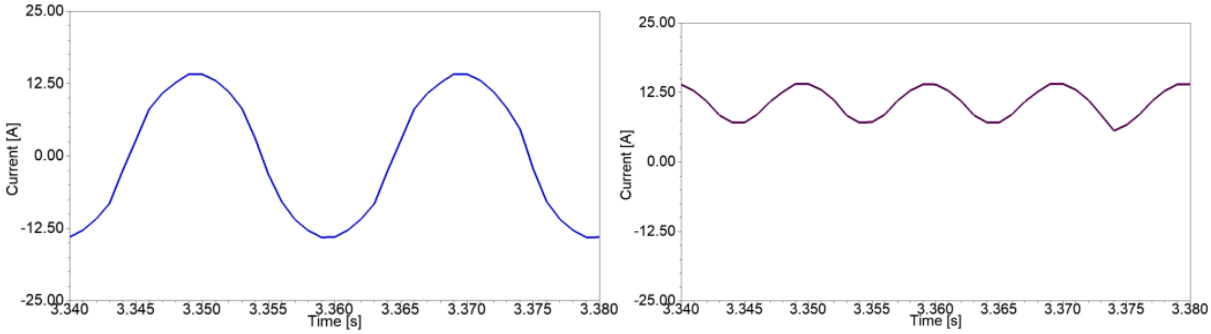

(a) Working current waveform at steady state (i_{AC}) *(b) Control current waveform at steady state (i_{DC})*

Fig. 22. Simulation results at U_{DC}=3.6 V

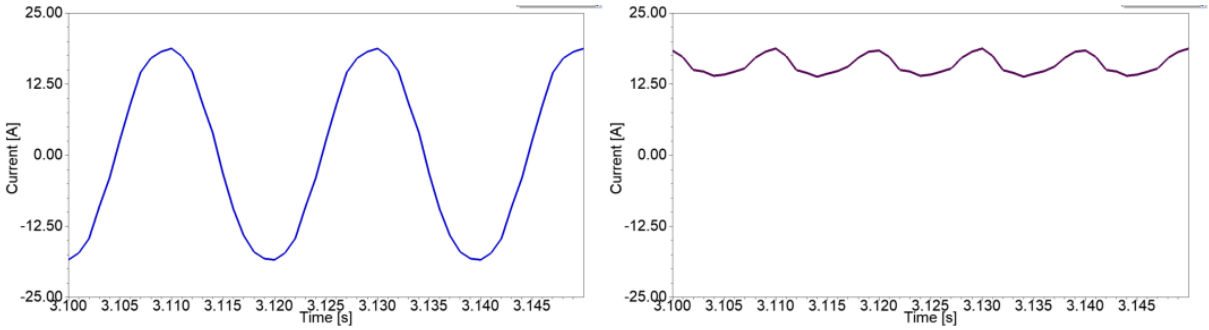

(a) Working current waveform at steady state (i_{AC}) *(b) Control current at steady state (i_{DC})*

Fig. 23. Simulation results at U_{DC}=5.41 V

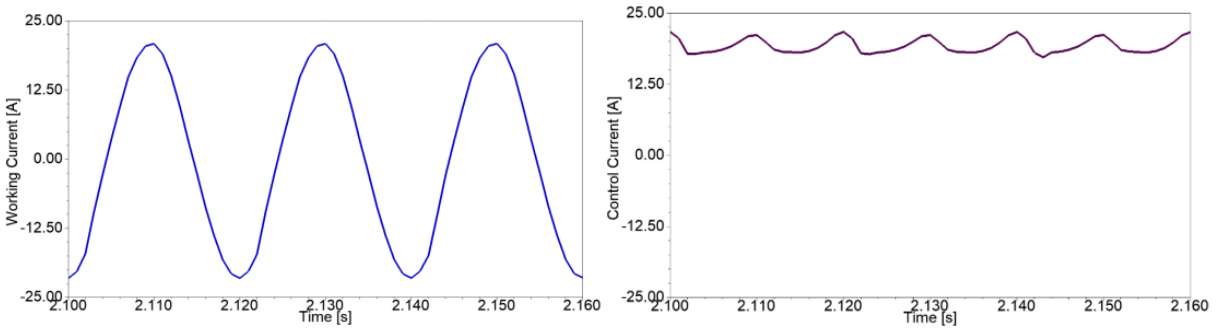

(a) Working current waveform at steady state (i_{AC}) *(b) Control current waveform at steady state (i_{DC})*

Fig. 24. Simulation results at U_{DC}=6.12 V

Table 2. Calculation results of the MCR model

U_{DC} (V)	i_{DC} (A)	i_{AC} (A)	α (0^O)	β (0^O)	B_{DC} (T)
0.000	0.00	0.00	180.00	0.00	0.00
0.19	0.54	1.04	160.00	76.48	0.09
0.72	2.11	3.76	140.00	123.10	0.23
1.53	4.51	7.38	120.00	163.52	0.38
2.53	7.45	11.06	100.00	200.68	0.52
3.60	10.58	14.17	80.00	235.60	0.65
4.59	13.52	16.33	60.00	269.00	0.75
5.41	15.92	17.52	40.00	300.00	0.82
5.94	17.49	17.97	20.00	331.00	0.87
6.12	18.03	18.03	0.00	360.00	0.88

Table 3. Simulation results of the MCR model

U_{DC} (V)	i_{DC} (A)	i_{AC} (A)	α (0^O)	β (0^O)	B_{DC} (T)
0.00	0.00	0.58	180.00	0.00	0.00
0.19	1.83	2.25	161.70	72.00	0.12
0.72	4.63	5.01	138.64	126.00	0.25
1.53	7.73	7.98	120.80	162.00	0.38
2.53	11.13	11.34	111.31	180.00	0.53
3.60	13.92	14.07	80.94	234.00	0.64
4.59	16.49	16.61	70.25	252.00	0.73
5.41	18.40	18.65	48.04	288.00	0.80
5.94	19.54	19.81	36.51	306.00	0.84
6.12	21.12	21.10	24.68	324.00	0.85

4. RESULTS. DISCUSSION

4.1. Analysis of MCR magnetic field distribution

The ultimate purpose of the magnetic controlled reactor with regards to regulating the grid voltage is achieved by adjusting the control winding current value to change the core magnetic saturation. Therefore, in order to obtain the accurate electromagnetic characteristics of the MCR, it is necessary to analyze the characteristics of each working state, and finally summarize if it is in conformity with electromagnetic characteristics of the MCR. The magnetic field distribution can effectively judge whether the simulation calculation result is accurate or not. In order to comprehensively analyze the magnetic field distribution of magnetic controlled reactor in the whole working interval, this paper mainly analyzes the four most critical stages of the magnetic field distribution of MCR.

Fig. 15 to *18* present magnetic field distribution inside the MCR core in a complete cycle during steady-state under different working conditions. The results of the simulation showed that magnetic flux distribution in the side yokes is uniform but nonuniform in the core limbs because of the magnetic valves in them. However, the introduction of these magnetic valves helps the MCR to function in the saturation region of the *B-H* magnetic characteristic curve.

It can be observed from *fig.15 (a)* and *(b)* that concentration of the magnetic flux is mostly in-between core limbs and side yokes, leaving the middle of the lower and upper yokes with least flux. In this instant, there is no DC excitation current in the control winding, so no DC flux is present and as a result, the core limbs mainly have AC flux produced by the working winding. Moreover, most of the AC flux circulates via the core limbs and side yokes, so the working winding reactive value is very large, allowing a very small amount of current to flow in the winding. In this case, the MCR is equivalent to an unloaded transformer, because both the core and magnetic valves are in an unsaturated state. The magnitude of magnetic flux density is almost 1.8T.

Fig. 16(a) and (b) show the influence of the superimposed magnetic field generated by the AC flux and the DC flux when 1.53 V was applied to the control winding. It can be observed that, in the first half cycle at time t =3.389s, the core limb I has more magnetic flux, followed by the left-side yoke, the right-side yoke and the core limb II respectively. This is because, at this moment, the AC voltage and current of the power supply are in positive and negative directions, and the DC excitation current is in the same direction with the AC on core limb I, which plays a role of enhancing magnetism, while the AC on core limb II is in opposite direction to the DC excitation current, which plays a role of demagnetization. Therefore, the magnetic valves on core limb I are largely in a saturated state, while the

magnetic valves on core limb II are still in an unsaturated state as expected. The magnetic flux density is obviously greater than 1.8T.

Fig. 17(a) and *(b)*, show the behavior of the magnetic flux in the second half cycle when the control voltage is still maintained at 1.53 V. It can be seen that at time t =3.399s, the magnetic flux on the core limb II is denser, followed by the right-side yoke, left-side yoke, and the magnetic flux on the core limb I is the least. This is because, over time, the AC reverses direction and follows the DC excitation current direction on core limb II, thereby, increasing the magnetization. At the same time, the AC on core limb I turns in the opposite direction to the DC excitation current, which leads to demagnetization. The magnitude of magnetic flux density is almost 2.1921T.

Fig.18 (a) and *(b)*, demonstrate the behavior of the magnetic flux when the control voltage is set to the half of the rated value, 3.6 V. It is obvious that at time t=3.355s, most of the magnetic flux is circulating between core limb I and core limb II. In this instant, there is no AC excitation current in the working winding, so no AC flux is present and as a result, most of the DC flux flow through core limb I and core limb II, and a small amount of DC flux flows through the side yokes. Thus, conforming to the principle of MCR.

4.2. Analysis of MCR control characteristics

The control characteristic refers to the correspondence between the working winding current and the control DC bias excitation of the magnetic controlled reactor.

Through the simulation, working winding current values of the MCR under different control DC bias excitations can be obtained.

The comparison between calculation and simulation of the MCR control characteristics is shown in Table 1 and 2 respectively. When the control angles of the calculation and simulation are at 0^0, the working winding current is at a maximum, and when both are at 180^0 the working winding current is at a minimum. This means that, in the range between 0^0 and 180^0, the output capacity of MCR can be smoothly regulated. It can also be seen from the same tables that when the control voltage value is 0 V, corresponding working current value with respect to the calculation is also 0.00 A, but the simulation current value is 0.58 A. This is because the calculation method is modeled based on an ideal situation while the simulation model adopted the actual working situation.

So, the simulation current value represents the magnetization current of the MCR under no-load condition. Again, it can be seen from *fig. 25* that the simulation current curve is slightly larger than that of the calculation curve. This is due to the small difference in the *B-H* curve data. Nevertheless, there is a good correlation among them and in line with the principle of MCR.

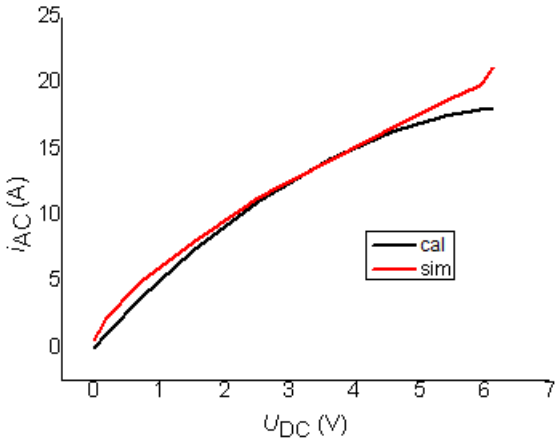

Fig. 25. Control characteristic curve of MCR

4.3. Analysis of MCR harmonics and time difference

It can be seen from *fig. 20* that when control winding current value is relatively small, the working winding current distortion is relatively large and the harmonic content is relatively high. As the control winding current increases, the working winding current waveform tends to be smooth with positive and cosine function waveform as shown in *fig. 21* to *24*. This is caused by the nonlinear magnetic properties of the ferromagnetic material. When the control current is relatively low, the MCR core works at the inflection point of the B-H magnetic characteristic curve, and the working winding current distortion rate is relatively high. It can also be seen that the steady-state period in *fig. 19* is the longest, followed by *fig.20, 21* to *24* respectively. This is possible because when the control excitation is low, the core operates below the inflection point of the B-H magnetic characteristic curve. But when control current starts to increase to a higher value, the time during which the core operates at the inflection point of the magnetic characteristic curve is decreasing continuously. At this juncture, the time for operating in the saturation state is due, and the distortion rate of the winding current waveform is decreased and appeared as a sine wave. This implies that for MCR working current to reach steady-state, harmonics and time vary in proportion to the control DC bias excitation.

4.4. Calculation and simulation of magnetic saturation degree results

The comparison between calculation and simulation of the MCR magnetic saturation degree is shown in *fig. 26*, it can be seen that the magnetic saturation curve measured by simulation is in good agreement with that of the calculation values. With the increase of control voltage from 2 V, the magnetic saturation degree obtained from calculation tends to be a little higher than that measured by the simulation. This is because assumptions were made in the calculation in arriving at idealizing the magnetic characteristic curve, while the simulation results exhibit the real working performance of the magnetic controlled reactor. However, there is a good correlation among them and in line with the principle of MCR.

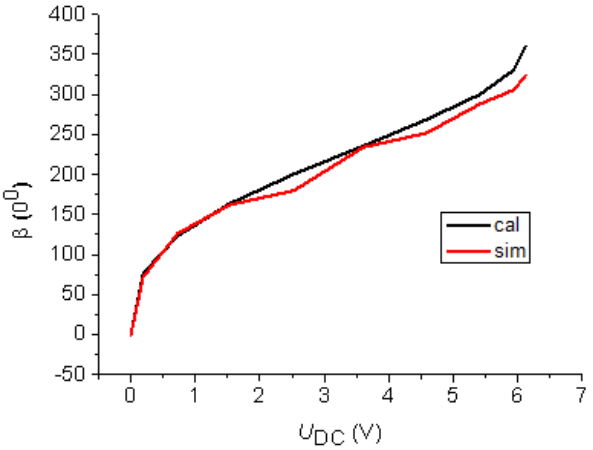

Fig. 26. Magnetic saturation degree of MCR

4.5. Analysis of MCR Inductance

The impedance of the MCR is $= U_{AC}/I_{AC}$. In reference to the data given and results of the simulation, reactance X_{L} is far bigger than winding resistance R_{A}, therefore, Z can be considered as X_{L}. The relationship between X_{L} and L is$X_L = \omega L = 2\pi f L$. The control DC bias excitation is varied in the range 0 V to 6.12 V, in which the change of inductance values is obtained as shown in *fig. 27*. It can be observed from the *fig.* that with the increase of control voltage the saturation degree of the core increases and the reactance value of the winding decreases. This is because the inductance of a coil is directly proportional to the permeability of its core material. When the voltage level of control winding increases to a certain extent, the core is completely saturated and the winding reactance value tends to be constant. It can also be seen from the same *fig.* that the inductance curve of the simulation is steeper than that of the calculation curve which truly reflects the difference in the *B-H* curve data. It is evidentiary from *fig. 27* that the AC inductance value equivalent of the working winding can be smoothly regulated with the change of the control DC bias excitation to achieve the purpose of adjusting the output capacity of the MCR. The simulation results are consistent with the theoretical analysis.

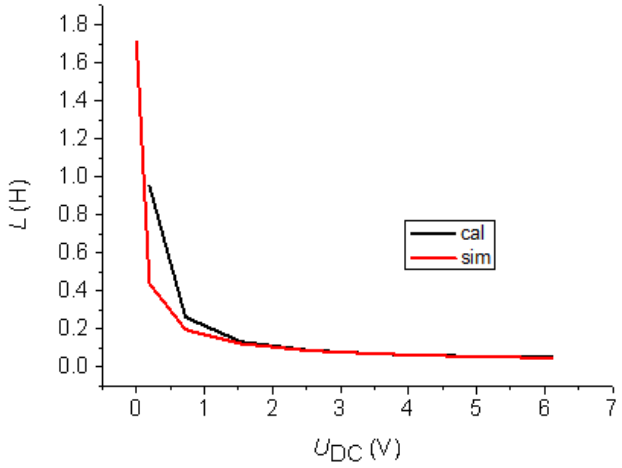

Fig. 27. Inductance curve of MCR

5. CONCLUSIONS

This paper mainly discussed the theoretical basis, structure, working principle and design model of a magnetic controlled reactor. The engineering simulation tool ANSYS Maxwell was used to establish the MCR model and calculate the magnetic field distribution and working characteristics.

Comparison of the calculation and simulation of the MCR model produced encouraging results under no-load to full-load working conditions. The results show that MCR alternately magnetize and demagnetize in between the left and right core limbs in one cycle which means that, the magnetic valves on both sides are alternately saturated and unsaturated in the cycle. At the same time, it has been verified that no matter how deep the magnetic valves saturate, no saturation phenomenon will occur in the core with large cross-section within the entire adjustable range. Therefore, the whole capacity of the MCR is smoothly adjusted by changing only the magnetic saturation degree of the magnetic valve core. The magnetic controlled reactor has approximately linear control characteristic curve, but when the current value of the control winding is increased to the rated value, the slope of the curve increases slowly and finally tends to a stable value. Through simulation and comparison, it is found that a small difference in the magnetic saturation characteristic curve can significantly affect the performance of MCR.

This research has given impetus to the understanding of MCR under actual operating condition. In addition, it has provided a vital basis for further research on the performance design of MCR.

REFERENCES

[1] T. Ben, L. Hou, L. Chen, P. Zhang, Y. Kong, R. Yan, *The Vector Electromagnetic Vibration of Magnetically Controlled Reactor Considering the Vector Hysteretic Magnetostriction Effect,* IEEE Transactions on Magnetics, vol. 58, 2022.

[2] A. V. R. Manuel, M. L. J. Vanessa, D. L. Cesar, *The Magnetically Controlled Reactor Applied to Peruvian Power System,* IEEE Latin America Transactions, vol. 18, pp. 1785 – 1792, 2020.

[3] A. V. Golovina, O. O. Pereslytskikh, A. S. Rodionova and A. N. Belyaev, *Analysis of Operation and Stability of Ultra-long Transmission Lines with Controlled Shunt Compensation,* in IEEE Conference of Russian Young Researchers in Electrical and Electronic Engineering (EIConRus), Russian, 2019.

[4] X. Gu, Y. Wu, T. Qu, W. Xu and D. Liu, *The simulation of the controllable reactor and it's application in Ultra High VoltageTransmission Lines,* in IEEE, Beijing, China, 2011.

[5] Z. Keju, W. Xin, B. He, *Research on Reactive Power Compensation Based on Magnetic*

Saturation Controllable Reactor, IEEE Access, vol 10, pp. 31377 – 31384, 2022.

[6] T. Ben, F. Chen, L. Chen, A. A. Siada, L. B. Jing, R. Yan, *Electromagnetic Vibration Analysis of Magnetically Controlled Reactor Considering DC Magnetic Flux*, IEEE Access, vol 8, pp. 170271 – 170280, 2020.

[7] L. L. S. D. Y. L. Wenye Liu, *Overview of Power Controllable Reactor Technology*, ELSEVIER Energy Procedia, vol. 17, no. Pt. A, pp. 483-491, 2012.

[8] A. Feshin and V. S. Chudny, *Transient stability of oil-field isolated power systems with magnetically controlled shunt reactors*, in 2016 IEEE NW Russia Young Researchers in Electrical and Electronic Engineering Conference (EIConRusNW), St. Petersburg, Russia, 2016.

[9] B. V. Oleksyuk, V. N. Tulsky and S. Palis, *Magnetically Controlled Shunt Reactors as Sources of Current and Voltage Harmonics*, IEEE Transactions on Power Delivery, vol. 33, no. 4, pp. 1818-1824, August 2018.

[10] E. Freedlander, *Static network stabilization—Recent progress in reactive power control*, GEC J, vol. 33, no. 2, pp. 58-65, 1966.

[11] H. Becker, *Die steuerbare Drosselspule. Ein statischer Phasenschieber zur Kompensation von Blindlaststosen*, ETZ-B23, vol. H.12, pp. 293-295, 1971.

[12] A. Bryantsev, *Magnetically Controlled Electrical Reactors*, Collection of Articles, 2012.

[13] Z. Shi-shuo, Y. Zhong-dong and P. Li, *Research of Magnetically Controlled Reactor*, in Proceedings of The 7th International Power Electronics and Motion Control Conference, Harbin, China, 2012.

[14] X. Chen, B. Chen and C. Tian, *A Novel Control Method for Magnetic-Valve Controllable Reactor*, in 2009 First International Workshop on Database Technology and Applications, IEEE, Wuhan, Hubei, China, 2009.

[15] J. Pei, T. Mingxing and Z. Huiying, *Winding Design and Control Method of A Novel Quick Response Magnetic-valve Controllable Reactor*, in 2019 22nd International Conference on Electrical Machines and Systems (ICEMS, Harbin, China, China, 2019.

[16] T. Mingxing, L. Qingfu and W. Shuhong, *An Equivalent Physical Model and a Mathematical Model of the MCR*, Transactions of China Electrotechnical Society, no. TM471, pp. 18-21+35, 08 2002.

[17] H. Zhang, M. Tian and P. Jing, *Effect of Magnetization Curve Model and Winding Connection Mode on Magnetically Saturated Controllable Reactor Based on ANSYS*, in 2019 22nd International Conference on Electrical Machines and Systems (ICEMS), Harbin, China, China, 2019.

[18] M. A. Khan, Z. Tao and L. Xiaoxiao, *Analysis of Faults and Protection Schemes for Magnetically Controlled Shunt Reactor*, in 2018 2nd IEEE Conference on Energy Internet and Energy System Integration (EI2), Beijing, China, 2018.

[19] M. Tümay, T. Demirdelen, S. Bal, R. İ. Kayaalp, B. Doğru and M. Aksoy, *A review of magnetically controlled shunt reactor for power quality improvement with renewable energy applications*, Renewable and Sustainable Energy Reviews, pp. 215-228, 12 04 2017.

[20] J. Dai, W. J, W. L, C. D, H. X and Z. W, *Reactive Power-Voltage Integrated Control Method Based on MCR*, in Proceedings of the 11th International Conference on Control Automation Robotics & Vision (ICARCV), 2010.

[21] Y. Po, Y. Zhongdong, C. Ruochen and K. Ning, *Analysis of Reactor Magnetic Circuit Based on ANSYS Command Flow*, Trans Tech Publications, Switzerland, Vols. 383-390, pp. 2256-2261, 22 11 2011.

[22] X. Cai and Y. Gao, Principle, *design and application of controllable saturable reactor*, Beijing: China Water Conservancy and Hydropower Press, 2008, pp. 3-5.

[23] F. Fiorillo, G. Bertotti, C. Appino and M. Pasquale, *soft magnetic materials*, J.Webster (ed.), Wiley Encyclopedia of Electrical and Electronics Engineering, pp. 1-42, 2016.

[24] Z. Lixia, *Mathematical analysis and Simulation of magnetic valve controllable reactor [Master 's Thesis]*, in Mathematical analysis and Simulation of magnetic valve controllable reactor [Master 's Thesis] , Beijing, North China Electric Power University, 2006, pp. 14-30.

[25] H. K. Chisepo, C. Guant and L. D. Borrill, *Measurements and FEM analysis of GIC/DC effects on transformer*, in IEEE PowerTech Milano, Milano, Italy, 2019.

[26] H. K. Chisepo, L. D. Borrill and C. T. Gaunt, *Measurements show need for transformer core joint details in finite element modelling of GIC and dc effects*, Compel International Journal of Computation and Mathematics in Electrical and Electronic Engineering, vol. 37, no. 3, pp. 1011-1028, 2018.

[27] T. Mingxing, Z. Qianru, Y. Jianning and L. Yibin, *Simulation and Analysis of Electromagnetic Transient Characteristics of Controllable Reactor of Transformer Type*, WSEAS Transactions on Circuits and Systems, vol. 14, 2015.

[28] C. Xuxuan, C. Baichao and T. Cuihua, *Two-stage saturable magnetically controlled reactor harmonic suppression optimization technique*,, Electric power automation equipment, vol. 31, no. 5, pp. 71-74, 2011.

[29] S. A. Darko, M. X. Tian and H. Y. Zhang, *Research on Magnetic-Valve Controllable Reactor Based on ANSYS*, International Journal of Recent Technology and Engineering (IJRTE), vol. 8, no. 3, pp. 671-675, September 2019.

[30] C. Baicao, T*heory and application of new controllable saturable reactor [M]*, Wuhan: Wuhan University of water conservancy and electric power press, 1999, pp. 45-73.

[31] W. Jun, Z. Hao, C. Baichao, L. WenHua, Y. ZhangTing, Z. ShengLong, Y. jiaxin and T. CuiHua, *Winding Loss Mechanism Analysis of Magnetic Valve Controlled Reactor*, International Journal of Control and Automation, vol. 9, no. 3, pp. 51-60, 2016.

[32] L. Yakun, *Research on Optimization of Dynamic Characteristics of Magnetic Control Reactor [D]*, Beijing : Beijing Jiaotong University, 2016, pp. 13-15.

[33] R. N. Jenipher and K. V. Chandrakala, *Magnetically controlled reactor based harmonic and voltage profile improvement in long transmission lines*, in 2017 Innovations in Power and Advanced Computing Technologies (i-PACT), IEEE, Vellore, India, 2017.